PHYSICS

Resolving the different bulk moduli within individual soft nanogels using small-angle neutron scattering

Judith Elizabeth Houston[1], Lisa Fruhner[2], Alexis de la Cotte[3], Javier Rojo González[3], Alexander Valerievich Petrunin[4], Urs Gasser[5], Ralf Schweins[6], Jürgen Allgaier[2], Walter Richtering[4,7], Alberto Fernandez-Nieves[3,8], Andrea Scotti[4]*

The bulk modulus, *K*, quantifies the elastic response of an object to an isotropic compression. For soft compressible colloids, knowing *K* is essential to accurately predict the suspension response to crowding. Most colloids have complex architectures characterized by different softness, which additionally depends on compression. Here, we determine the different values of *K* for the various morphological parts of individual nanogels and probe the changes of *K* with compression. Our method uses a partially deuterated polymer, which exerts the required isotropic stress, and small-angle neutron scattering with contrast matching to determine the form factor of the particles without any scattering contribution from the polymer. We show a clear difference in softness, compressibility, and evolution of *K* between the shell of the nanogel and the rest of the particle, depending on the amount of cross-linker used in their synthesis.

INTRODUCTION

Soft and compressible colloids are often the building blocks of many of the systems used in soft matter. Due to their softness, an increase in concentration, which consequently increases the suspension osmotic pressure, π, causes the particles to either change their volume by isotropically shrinking (*1*–*3*) or change their shape by faceting (*3*–*6*). To disentangle these effects, it is crucial to know the particle bulk modulus, $K = -v\frac{\partial \pi}{\partial v}$, which quantifies the resistance of the material to isotropically changing its volume. Another complication arises from the fact that, often, these nanosized soft colloids have complex internal architectures. For example, viruses consist of a viral capsid containing genetic material in different phases (*7*). Both the capsid and the DNA phases are expected to have different softness, and both are expected to play a role in virus infectivity (*8*, *9*), as well as in how they adhere to host interfaces (*10*, *11*). Microgels (*12*) and nanogels (*13*) are one of the most commonly-used model systems to study the effects of particle compressibility on both phase transitions, crowding (*2*), and flow behavior (*14*–*16*). Similar to viruses, they often also have a core region that is distinct from a surrounding fuzzy shell (*4*, *17*–*19*).

In all these cases, it is natural to expect that an overall value of the elastic modulus is insufficient to predict the deformation behavior of the particles and that local values of *K* in relation to their internal structure are more appropriate. In addition, it is typical that the more a soft colloid is compressed, the more it stiffens (*20*). The associated nonlinear behavior then demands knowing *K* as a function of strain. Being able to quantify this dependence, and doing it locally to account for the internal structure of the particles, is challenging, rendering any existent methodology to obtain *K* insufficient.

Current methodologies include using osmotic stress polymers to deswell the particle while measuring its size and shape with optical microscopy (*21*, *22*). For sufficiently large objects, one could alternatively use capillary micromechanics and microfluidics (*23*). However, both these methods fail for particles in the size range of viruses, nanoparticles, colloidal nanogels, and macromolecules.

An alternative strategy that, in principle, allows probing the compression of nanosized colloids is to use light scattering. In this case, because the polymer used to osmotically stress the particles must have a high molecular weight, M_w, to prevent its penetration inside the particles (*24*, *25*), both soft colloids and polymers contribute to the scattering signal in water-based environments, which are particularly interesting in biologically relevant studies. This often makes it impossible to disentangle the contribution from each of the two, thus preventing the determination of the nanogel size (*25*).

Here, we probe the local bulk moduli and their evolution with compression for nanogels, which we use as a model system of compressible nanosized colloids with complex internal architecture. Small-angle neutron scattering (SANS) with contrast variation is used to probe the form factors of poly-*N*-isopropylacrylamide (pNIPAM)–based nanogels and to resolve the changes in their architecture once compressed by partially-deuterated polyethylene glycol (PEG) that can be contrast-matched to the solvent. For the stressing polymer, we synthesized PEG with a number-average molecular weight M_n= 265,000 g/mol and a deuteration degree of 83%, $d_{83\%}$PEG, so that it can be contrast-matched to the solvent D_2O as discussed in section S1 and shown in fig. S1. Therefore, by using neutrons rather than light, we can disentangle the particle and $d_{83\%}$PEG signals, extending the conditions under which the particle size and, hence, its bulk modulus can be determined. Furthermore, because we can also determine how the dimensions associated with the internal particle structure change with osmotic pressure, we can obtain the bulk modulus of these various parts separately and how they vary with the imposed stress. We do this with ultralow cross-linked (ULC) nanogels and with nanogels containing 1 and 5 mole percent (mol %) of cross linker.

[1]European Spallation Source ERIC, Box 176, SE-221 00 Lund, Sweden. [2]Forschungszentrum Jülich GmbH Jülich Centre for Neutron Science (JCNS-1) and Institute for Biological Information Processing (IBI-8), 52425 Jülich, Germany. [3]Department of Condensed Matter Physics, University of Barcelona, 08028 Barcelona, Spain. [4]Institute of Physical Chemistry, RWTH Aachen University, 52056 Aachen, Germany. [5]Laboratory for Neutron Scattering and Imaging, Paul Scherrer Institut, 5232 Villigen, Switzerland. [6]Institut Laue-Langevin ILL DS/LSS, 71 Avenue des Martyrs, F-38000 Grenoble, France. [7]JARA-SOFT, 52056 Aachen, Germany. [8]ICREA-Institucio Catalana de Recerca i Estudis Avancats, 08010 Barcelona, Spain.
*Corresponding author. Email: andrea.scotti@rwth-aachen.de

RESULTS

We determine the form factors of single nanogel particles by preparing dilute suspensions in the presence of partially-deuterated PEG ($d_{83\%}$PEG) used as stressing polymer at different concentrations. We use both $d_{83\%}$PEG (see section S1) and ULC and cross-linked nanogels (see section S2). The solvent consists of heavy water that is contrast-matched to $d_{83\%}$PEG, which, as a result, does not contribute to the SANS signal. Consistent with this, the overall shape of the SANS data agrees with that expected from dilute solutions of spherical objects (see Fig. 1). Note the absence of a peak in the low-q region, suggesting that the suspension structure factor is essentially one and that the scattered intensity, $I(q)$, is due to the nanogel form factor only. We also note that the radius of gyration of $d_{83\%}$PEG, measured using light scattering, is 25 nm in agreement with predictions in the literature for PEG with comparable M_w (see section S1) (*26*), which is larger than the largest mesh size of the nanogels used here and that corresponds to 12 nm; this ensures that $d_{83\%}$PEG does not penetrate the nanogel particles. We find that the shoulder in $I(q)$ shifts to progressively higher q values with increasing $d_{83\%}$PEG concentration and, thus, increasing osmotic pressure, π (see fig. S2 in section S3). Concomitantly, the slope of the scattering curves in the low-q region decreases with increasing π. Both these facts indicate that the nanogels are progressively compressing (*2*).

To quantitatively estimate the size change and gain insight into the variation of the internal structure of the nanogels as they compress, we fit the data using a fuzzy sphere model for the form factor (see eq. S6 in section S4). This model accounts for the internal architecture of nanogels having a homogeneous core of radius R_c, surrounded by a fuzzy shell that is approximated by a Gaussian of width 2σ. We note that it is difficult to sharply define a core and a shell. However, any analysis of scattering data requires a model, and all reasonable models used to describe nanogels assume some kind of size for a core and another for a shell (*13*, *27*–*29*). In the fuzzy sphere model that we use, the extension of the core region has a radius equal to R_c, and the shell has a length of 2σ. The total radius of the particle is thus $R = R_c + 2\sigma$ (*13*).

Recently, more complicated models have been developed to fit the SANS data of nanogels composed of different polymers, or with a hard incompressible core or a solvent-filled cavity in their center (*19*, *27*, *28*). However, there is unanimous agreement in the literature that, for pNIPAM-based nanogels with cross-linking concentration up to 5 mol %, all these new models lead to virtually the same results as the fuzzy sphere model (*27*–*29*). Therefore, we use the latter to fit our data.

The fits of the data using this model correctly describe the data, as shown by the solid curves in Fig. 1; note that this is true for all three nanogels. In section S6, we show that using a model that does not rely on a defined internal architecture leads to virtually the same fits and characteristic lengths. Furthermore, in the same section, we show that the trend of π with both the fitting parameter associated with the size polydispersity in the fuzzy shell model and the fitting of the data with an elliptical model does not show any signs of asphericity of the nanogel even for the highest compressions.

From the fits, we determine both the core and shell dimensions and, thus, the nanogel radius, R. Consistent with the shape evolution of the scattering curves, we find that R, normalized with the nanogel radius in the absence of free polymer, R_0, monotonically decreases with increasing π; this is shown for the ULC (circles), the 1 mol % cross-linked nanogels (diamonds), and 5 mol % cross-linked nanogels (squares) in Fig. 2A. We consider relative variations of the radii smaller than 2% to be within experimental error and not due to the effect of the osmotic stress applied by the $d_{83\%}$PEG. Therefore, a significant change in size is registered at $\pi = (0.1843 \pm 0.0007)$ kPa for the ULC nanogels, at $\pi = (0.839 \pm 0.002)$ kPa for the 1 mol % cross-linked nanogels, and at $\pi = (29.95 \pm 0.03)$ kPa for the 5 mol % cross-linked nanogels. These points are highlighted with arrows in Fig. 2. These values are an approximate initial estimate of K; the resolution here is limited by the number of samples we have been able to measure on the SANS beamlines.

We then compute the nanogel volume $v = 4\pi R^3/3$ from the size, R (table S1), and correlate it with π (see Fig. 2B). The relative slopes of these curves then provide the bulk modulus, K, which we show as a function of the relative nanogel volume in Fig. 2C. The values of the local K are obtained considering only two adjacent points, j and $j + 1$, and the compression of the nanogel with initial volume v_j. The errors, are computed using error propagation. The advantage of this approach is that we access the local bulk modulus of the nanogels and study its evolution with compression. However, reliable

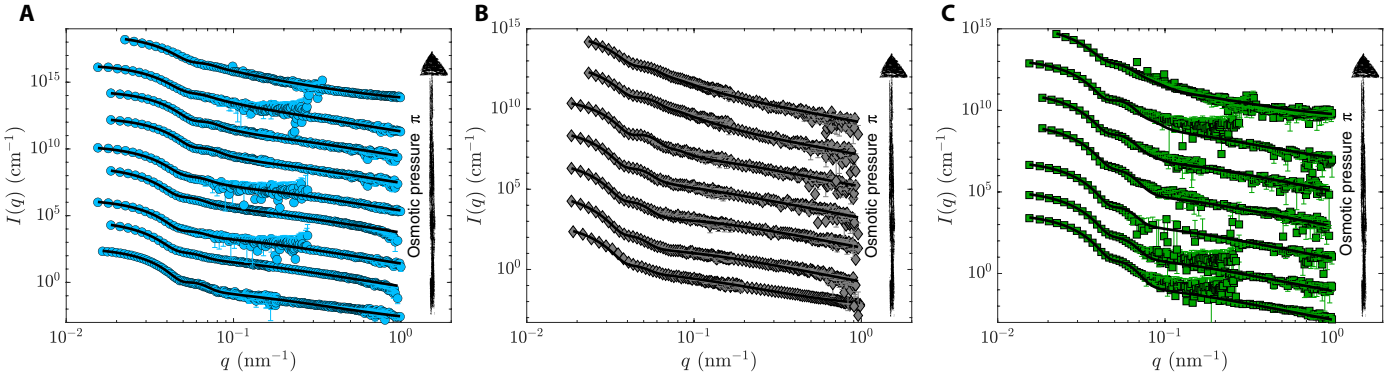

Fig. 1. SANS measurements of soft to harder nanogels with increasing osmotic pressure. SANS intensity, $I(q)$, as a function of the scattering vector, q, of the (**A**) ULC nanogels, (**B**) 1 mol % cross-linked nanogels, and (**C**) 5 mol % cross-linked nanogels probed at 20.0° ± 0.1°C in pure D_2O. The osmotic pressure exerted by the $d_{83\%}$PEG are from the bottom to top: in (A), 0, 0.0604 ± 0.0005, 0.1840 ± 0.0007, 0.358 ± 0.002, 1.053 ± 0.002, 2.797 ± 0.006 28.65 ± 0.03, 72.19 ± 0.05, and 158.89 ± 0.09 kPa; in (B), 0, 0.178 ± 0.001, 0.839 ± 0.002, 4.753 ± 0.009, 32.20 ± 0.03, 69.10 ± 0.05, and 128.74 ± 0.08 kPa; and in (C), 0, 0.184 ± 0.001, 1.053 ± 0.002, 2.797 ± 0.006, 29.95 ± 0.03, 71.01 ± 0.05, and 120.17 ± 0.07 kPa. The solid lines are fits of the data with the model for a fuzzy sphere (*13*). Data are shifted in the y direction for clarity by 10^{2i}, where i is the number of the curves from the bottom to top starting from 0. The bottom curves in (A) to (C) are unshifted and, therefore, in absolute units.

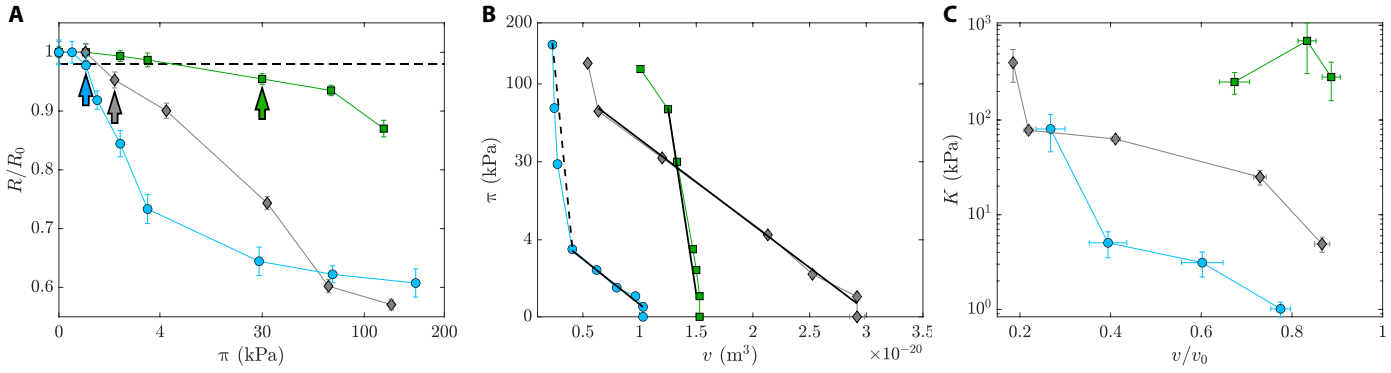

Fig. 2. Evolution of the nanogels' sizes and bulk moduli. (**A**) Variation of the radius normalized for the radius measured at π = 0 kPa, *R*/*R* (π = 0) kPa, versus π. (**B**) Osmotic pressure of the suspensions, π, versus nanogel volume, *v*. (**C**) Evolution of the nanogel bulk modulus as a function of compression expressed by the ratio between the volume and the volume of the nanogel in the swollen state. Circles represent data relative to ULC nanogels, diamonds correspond to the regular 1 mol % cross-linked nanogels, and the regular 5 mol % cross-linked nanogels are represented by squares. The arrows indicate the values of *K* for the initial shrinking we are able to detect.

results are obtained only if the change in volume is large enough compared to the error in the volume change. This error is of the order of 10^{-22} m^3, which is of the same order of magnitude of the change in volume for small volume changes. In this case, the error in the local value of *K* is very large. In particular, the points relative to the early compression of the 5 mol % cross-linked nanogels, and the values corresponding to the highest applied osmotic stress for the ULC and 1 mol % cross-linked nanogels, are affected by large errors.

Our results confirm that the ULC nanogels are the softest. We find K_{ULC} = (1.0 ± 0.2) kPa and $K_{1\ \mathrm{mol\%}}$ = (4.9 ± 0.3) kPa. In addition, $K_{5\ \mathrm{mol\%}}$ = (284 ± 124) kPa. The large value in *K* for the 5 mol % cross-linked nanogels implies that we can only obtain reliable values for the bulk modulus at higher compressions, where some of the pNIPAM would already have rearranged in the nanogel volume, leading to an increased *K*.

As the osmotic pressure increases, *K* also increases, indicating that the nanogels progressively become stiffer. This can be understood from the fact that compressing the particles leads to solvent expulsion and to a concomitant increase in pNIPAM density (*20*). For the 5 mol % cross-linked nanogels, we are able to achieve a maximum compression of ≈67% relative to the volume in the absence of $d_{83\%}$PEG. The local value of *K* remains almost unchanged within experimental error. Higher compressions are achieved for both the ULC and the 1 mol % cross-linked nanogels. In these cases, the smallest volumes obtained are ≈20 to 25% of the volume in the absence of $d_{83\%}$PEG.

As expected, the values of *K* for the cross-linked nanogels are generally larger than those for the ULC nanogels. At the maximum π applied, the value of *K* for the ULC nanogels is (80 ± 34) kPa, while it is (403 ± 153) kPa for the 1 mol % cross-linked nanogels. Therefore, even in a highly compressed state, the ULC nanogel remains the softest. The large value for the bulk modulus of the 1 mol % of cross-linked nanogels might reflect the incompressibility of their cross-linked core.

The values of the initial bulk moduli we determine are consistent with the values reported in the literature for nanogels with comparable swelling behavior, as determined by dynamic light scattering (*25*), capillary micromechanics and microfluidics (*23*), and osmotic stress solutions (*30*) (see section S7). Regarding the increase in approximately two orders of magnitude of *K* with compression, there are not comparable data in the literature, because only with the use of SANS with contrast variation and $d_{83\%}$PEG, as we propose, can one reach high-enough π to detect the increases in *K*. However, an increase in the Young's modulus comparable to the one measured for our 5 mol % cross-linked nanogels is reported in the literature for nanogels with a comparable swelling degree (see table S2) (*31*, *32*).

In addition to the local variation in *K*, we also compute an average bulk modulus for the whole particle. This is done by performing a fit on the series of points that vary linearly in Fig. 2B; these are shown as solid and dashed lines. The slopes of these fits are multiplied by $-v$ to obtain the value of *K*, where *v* is the volume of the swollen nanogel. The values we obtain can be seen as an average value of the bulk moduli of the particle. As can be seen, the ULC nanogels show two compression regimes fitted by the solid and dashed lines. The initial average bulk modulus is (2.4 ± 0.3) kPa, while, in the second regime, the average bulk modulus becomes $\langle K_{\mathrm{ULC}} \rangle$ = (12 ± 1) kPa. For both the cross-linked nanogel, we can identify only one main compression regime. The fits of these data leads to $\langle K_{1\ \mathrm{mol\%}} \rangle$ = (6.5 ± 0.4) kPa and $\langle K_{5\ \mathrm{mol\%}} \rangle$ = (30.0 ± 0.5) kPa.

Together with the possibility to reach unprecedentedly high π, thanks to contrast variation, the use of neutron scattering also allows us to determine the characteristic lengths within the nanogel. We find that, for low π, the compression of the fuzzy shell, shown in Fig. 3A, mimics the overall compression of the particles, shown in Fig. 2A. The first compression detectable (see arrows in Fig. 3B) for the ULC and 1 mol % cross-linked nanogels happens at the same values detected in Fig. 2, and, therefore, these values can be considered as the initial bulk modulus of the shell, K_s. In contrast, the fuzzy shell of the 5 mol % of cross-linked nanogels shows a significant change in size at π = (2.797 ± 0.006) kPa.

However, for some π, the shell of the ULC nanogels abruptly collapses, becoming indistinguishable from zero for π ≳ 4 kPa. For the 1 mol % cross-linked nanogels, this happens for π ≳ 32 kPa, but the decrease in σ is more gradual compared to the abrupt decrease seen for the ULC nanogels (see Fig. 3A). This confirms that the fuzzy shell of these cross-linked nanogels is more cross-linked than that of ULC nanogels. For the 5 mol % cross-linked nanogels, the shell shrinks even more progressively than for the 1 mol % cross-linked nanogels, compressing it to about ≈53% of its initial volume at the highest π we apply (see Fig. 3A).

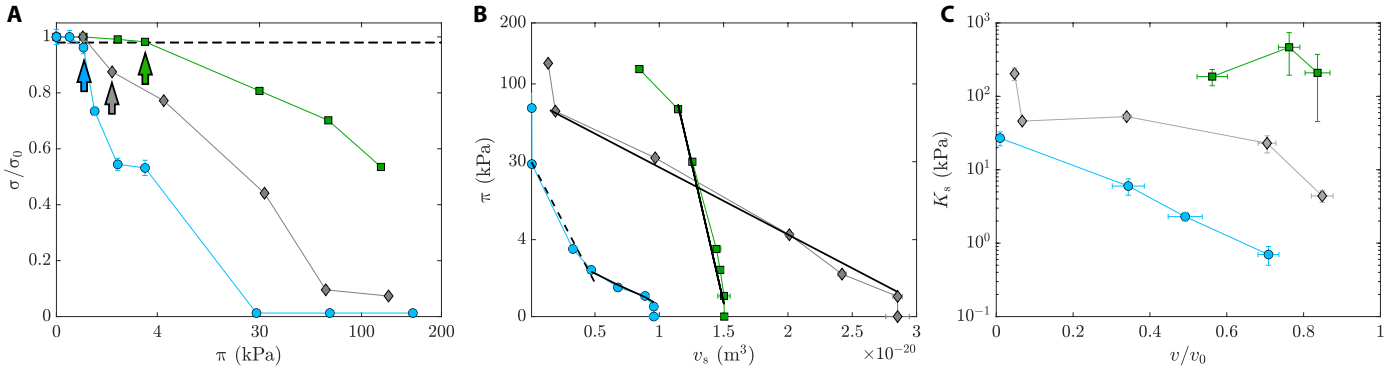

Fig. 3. Evolution of the thicknesses and bulk moduli of the nanogels' shells. (**A**) Variation of the shell thickness normalized for the shell thickness measured at π = 0 kPa, 2σ/2σ (π = 0 kPa), versus π. (**B**) Suspension osmotic pressure, π, versus shell volume, v_s. (**C**) Evolution of the shell bulk modulus as a function of compression expressed by the ratio between the volume of the shell and the volume of the shell in the swollen state. Circles represent data relative to ULC nanogels, diamonds correspond to the regular 1 mol % cross-linked nanogels, and the regular 5 mol % cross-linked nanogels are represented by squares.

In Fig. 3B, as we did for the whole nanogel, we correlate π with the shell volume, $v_s = 4\pi/3(R^3 - R_c^3)$; R and R_c are the values of the radius of the total particle and of the core, as obtained from the SANS fits and listed in table S1. Then, the bulk modulus of the shell, K_s, is obtained from the local slopes of the curves and plotted in Fig. 3C. Note that K_s is a crucial parameter that greatly affects interparticle interactions at high packing fractions (*16*, *33*–*35*); it was used in advanced multi-Hertzian models for the interaction potential to reproduce experimental structure factors of concentrated nanogel suspensions (*15*). The evolution of K_s with particle compression reflects that the more the fuzzy shell is compressed, the harder it becomes. Note, however, that $K_s < K$. In particular, at low π, we find $K_s = (0.7 \pm 0.2)$ kPa for the ULC nanogels, $K_s = (4.4 \pm 0.2)$ kPa for the 1 mol % cross-linked nanogels, and $K_s = (209 \pm 163)$ kPa for the 5 mol % cross-linked nanogels. This implies that, in all cases, the initial change in size is due to the compression of the shell, which is the softest. We note, however, that, for the 5 mol % cross-linked nanogels, the small change in volumes leads again to very large values of K with a large uncertainty. Therefore, as before, we can also make linear fits in Fig. 3B to obtain the average values of the shell bulk modulus, $\langle K_s \rangle$. These fits are shown as solid lines. With this approach, $\langle K_{s,ULC} \rangle$ equals (1.8 ± 0.2) kPa for the initial compression of the ULC and then rises up to (4.2 ± 0.3) kPa. For the 1 and 5 mol % cross-linked nanogels, we find single average values $\langle K_{s,1\ mol\%} \rangle = (2.6 \pm 0.2)$ kPa and $\langle K_{s,5\ mol\%} \rangle = (19 \pm 2)$ kPa, respectively.

DISCUSSION

Our work presents a method for quantifying the different bulk moduli, and their evolution with compression, within soft compressible nanosized colloids with complex internal architectures. We have developed a route to obtain a high molecular weight, partially-deuterated PEG with a narrow molecular weight distribution. This process is new to the best of our knowledge. This partially-deuterated PEG is used to exert osmotic stress on nanogel particles, which is to be taken as a model system of other soft compressible colloids. The form factor of the particles was then measured using SANS. As the partially-deuterated PEG is contrast-matched with the solvent, the SANS data are directly related to the size and structure of the particles, without any contributions from the $d_{83\%}$PEG. This allowed the bulk moduli of the particles as a whole to be obtained and that of the different morphological regions within the particles, especially the external soft shell. Our results indicate that the bulk modulus of the fuzzy shell is significantly smaller than the overall bulk modulus of the particles and that both of them increase with cross-linker concentration.

Our approach can be applied to other soft colloids in suspension. The use of neutrons has two major advantages: Samples can be studied in situ in an aqueous environment, with only the addition of heavy water to contrast-match the partially deuterated PEG. Nevertheless, note that the substitution of water with heavy water may have an effect on the properties of the system; for instance, it may shift the volume phase transition temperature of thermosensitive polymers such as pNIPAM (*36*) or slow down the rate of chemical reactions and biological processes (*37*). This effect, however, should not significantly modify particle compressibility. Thus, our method should be applicable to biologically relevant macromolecules and colloids. For example, because the internal osmotic pressure of the genetic material within a viral capsid and the stiffness of the capsid both play a key role in virus infectivity (*8*, *9*), we envision using our methodology to probe the structure of the capsid and the internal compressibility of the genetic material, and doing this for both natural viruses (*38*) and virus-like colloids (*39*, *40*). In addition, we expect our methodology to enable determining the stiffness of macromolecules, such as DNA, and of DNA assemblies or DNA origami (*41*, *42*). This is of particular interest because DNA stiffness plays a role in its denaturation (*43*), as well as in its packing inside the nucleosome (*44*).

Last, we emphasize that the use of partially-deuterated high molecular weight PEGs is not limited to osmotic stress experiments. High–molecular weight PEGs find important applications in the biomedical sciences. They are used, for example, in pharmaceutical formulations, such as therapeutic proteins (*45*) and as lubricants (*26*), e.g., in total joint replacements (*46*). Therefore, exploiting our synthetic procedures, we envisage future experiments harnessing deuterated PEGs and neutron scattering with contrast variation to isolate in situ the dynamic structure of the material of interest.

MATERIALS AND METHODS

Partially deuterated PEG ($d_{83\%}$PEG)

The partially-deuterated PEG ($d_{83\%}$PEG) was synthesized according to the procedure described in section S1.2. Briefly, the initiator, low molecular weight–deuterated PEG (dPEG600; M_n = 645 g/mol) was metalated to a degree of about 90% with potassium *tert*-butoxide in dry benzene. The metalated initiator was then polymerized in toluene, and a 11:2 mixture of ethylene oxide-d_4 and hydrogenous ethylene oxide for 3 days. A polymer was obtained with a D/H composition of 83%, as determined by ^{1}H nuclear magnetic resonance spectroscopy. SANS measurements show that, as expected, $d_{83\%}$PEG is virtually completely contrast-matched in pure D_2O (see section S1.3). The final product of $d_{83\%}$PEG had number-average molecular weight, M_n, of 265,000 g/mol and molecular weight distribution, M_w/M_n, of 1.02.

Suspension preparation

A stock solution of $d_{83\%}$PEG in pure heavy water is realized with the $d_{83\%}$PEG at a concentration of $c_{d83\%PEG}$ = (8.424 ± 0.002) wt %. Samples are then prepared from this stock solution by dilution with both heavy water and nanogel solutions at a concentration $c_m \simeq$ 0.355 wt % in pure D_2O. To minimize the error in the concentration of all samples, they were prepared by weighing $d_{83\%}$PEG, pNIPAM, and D_2O using a balance (Mettler Toledo, XP205) with a resolution of 10^{-5} g. In this way, a series of samples containing the nanogels at a constant packing fraction $\lesssim$0.03 is realized. The concentration of $d_{83\%}$PEG in these samples varies between 6.5 and 0.25 wt %.

Osmotic pressure measurements

The osmotic pressure $d_{83\%}$PEG solutions with concentrations between 0.1 and 4 wt % were measured using a membrane osmometer (Wescor, 4420). Measurements of samples at higher concentration and, therefore, higher viscosity were not possible. The instrument consists of two chambers, separated by a semipermeable membrane. In one chamber, named sample chamber, the sample whose osmotic pressure we want to know is injected. The other chamber, named reference chamber, is filled with the solvent used for the solution, in our case, heavy water. The reference chamber is coupled to a transducer that converts mechanical pressure into an electrical signal that is then transformed into a pressure value (*47*).

Small-angle neutron scattering

The measurements have been performed using two SANS instruments, SANS-I at the Paul Scherrer Institut (Villigen, Switzerland) and D11 at the Institut Laue-Langevin (Grenoble, France). SANS-I has been operated using a neutron wavelength λ = 1.1 nm for the sample-to-detector distance d_{SD} = 18 m, and a λ = 0.5 nm for d_{SD} = 6 m. D11 has been operated at a constant λ = 0.6 nm for d_{SD} = 28, 5.5, and 1.7 m. SANS-I has a ^{3}He detector with a pixel size of 7.5 mm by 7.5 mm. While D11 has Stokes multitube arrays with pixels of 4 mm by 8 mm. The error in wavelength selection is Δλ/λ = 10%. All measurements were performed at a constant temperature of (20.0 ± 0.1)°C.

All the suspensions were prepared in pure D_2O to contrast-match the scattering length density of the $d_{83\%}$PEG and the solvent. In this way, the contribution to the scattering signal of $d_{83\%}$PEG is masked and the scattered intensity depends only on the size and internal architecture of the hydrogenated nanogels in solution. A similar approach that uses deuterated nanogels instead of $d_{83\%}$PEG to create an "invisible" matrix with a few interspersed hydrogenated nanogels that are embedded has been largely used to access the response of nanogels with different internal architecture and sizes to crowding (*2*, *48*). These nanogels come from the same batches of the nanogels used in the literature (*19*, *49*, *50*). More information about the precipitation polymerization synthesis can be found in section S2 and in (*19*, *49*, *50*).

SUPPLEMENTARY MATERIALS

Supplementary material for this article is available at https://science.org/doi/10.1126/sciadv.abn6129

REFERENCES AND NOTES

1. A. Carlsen, N. Glaser, J.-F. Le Meins, S. Lecommandoux, Block copolymer vesicle permeability measured by osmotic swelling and shrinking. *Langmuir* **27**, 4884–4890 (2011).
2. A. Scotti, U. Gasser, E. S. Herman, M. Pelaez-Fernandez, L. A. Lyon, A. Fernandez-Nieves, The role of ions in the self-healing behavior of soft particle suspensions. *Proc. Natl. Acad. Sci. U.S.A.* **113**, 5576–5581 (2016).
3. J. Zhang, P. M. Lettinga, J. K. Dhont, E. Stiakakis, Direct visualization of conformation and dense packing of DNA-based soft colloids. *Phys. Rev. Lett.* **113**, 268303 (2014).
4. G. M. Conley, P. Aebischer, S. Nöjd, P. Schurtenberger, F. Scheffold, Jamming and overpacking fuzzy microgels: Deformation, interpenetration, and compression. *Sci. Adv.* **3**, e1700969 (2017).
5. C. K. Wong, M. H. Stenzel, P. Thordarson, Non-spherical polymersomes: Formation and characterization. *Chem. Soc. Rev.* **48**, 4019–4035 (2019).
6. V. Kozlovskaya, M. Dolmat, E. Kharlampieva, Polymeric particulates of controlled rigidity for biomedical applications. *ACS Appl. Polym. Mater.* **3**, 2274–2289 (2021).
7. A. Minsky, E. Shimoni, D. Frenkiel-Krispin, Stress, order and survival. *Nat. Rev. Mol. Cell Biol.* **3**, 50–60 (2002).
8. P. J. P. Carrillo, M. Medrano, A. Valbuena, A. Rodriguez-Huete, M. Castellanos, R. Perez, M. G. Mateu, Amino acid side chains buried along intersubunit interfaces in a viral capsid preserve low mechanical stiffness associated with virus infectivity. *ACS Nano* **11**, 2194–2208 (2017).
9. S. Bhatia, L. C. Camacho, R. Haag, Pathogen inhibition by multivalent ligand architectures. *J. Am. Chem. Soc.* **138**, 8654–8666 (2016).
10. C. Riekel, M. Burghammer, I. Snigirev, M. Rosenthal, Microstructural metrology of tobacco mosaic virus nanorods during radial compression and heating. *Soft Matter* **14**, 194–204 (2018).
11. M. Hernando-Pérez, C. Zeng, M. C. Miguel, B. Dragnea, Intermittency of deformation and the elastic limit of an icosahedral virus under compression. *ACS Nano* **13**, 7842–7849 (2019).
12. R. Pelton, P. Chibante, Preparation of aqueous latices with N-isopropylacrylamide. *Colloids Surf.* **20**, 247–256 (1986).
13. M. Stieger, W. Richtering, J. S. Pedersen, P. Lindner, Small-angle neutron scattering study of structural changes in temperature sensitive microgel colloids. *J. Chem. Phys.* **120**, 6197–6206 (2004).
14. J. Mattsson, H. M. Wyss, A. Fernandez-Nieves, K. Miyazaki, Z. Hu, D. R. Reichman, D. A. Weitz, Soft colloids make strong glasses. *Nature* **462**, 83–86 (2009).
15. M. J. Bergman, N. Gnan, M. Obiols-Rabasa, J. M. Meijer, L. Rovigatti, E. Zaccarelli, P. Schurtenberger, A new look at effective interactions between microgel particles. *Nat. Commun.* **9**, 5039 (2018).
16. G. M. Conley, C. Zhang, P. Aebischer, J. L. Harden, F. Scheffold, Relationship between rheology and structure of interpenetrating, deforming and compressing microgels. *Nat. Commun.* **10**, 2436 (2019).
17. M. Keerl, J. S. Pedersen, W. Richtering, Temperature sensitive copolymer microgels with nanophase separated structure. *J. Am. Chem. Soc.* **131**, 3093–3097 (2009).
18. F. Scheffold, Pathways and challenges towards a complete characterization of microgels. *Nat. Commun.* **11**, 4315 (2020).
19. A. Scotti, S. Bochenek, M. Brugnoni, M. A. Fernandez-Rodriguez, M. F. Schulte, J. E. Houston, A. P. H. Gelissen, I. I. Potemkin, L. Isa, W. Richtering, Exploring the colloid-to-polymer transition for ultra-low crosslinked microgels from three to two dimensions. *Nat. Commun.* **10**, 1418 (2019).
20. P. van der Scheer, T. van de Laar, J. van der Gucht, D. Vlassopoulos, J. Sprakel, Fragility and strength in nanoparticle glasses. *ACS Nano* **11**, 6755–6763 (2017).
21. V. Kozlovskaya, B. Xue, M. Dolmat, E. Kharlampieva, Complete pH-dependent shape recovery in cubical hydrogel capsules after large osmotic deformations. *Macromolecules* **54**, 9712–9723 (2021).
22. C. Gao, E. Donath, S. Moya, V. Dudnik, H. Möhwald, Elasticity of hollow polyelectrolyte capsules prepared by the layer-by-layer technique. *Eur. Phys. J. E* **5**, 21–27 (2001).

23. P. Voudouris, D. Florea, P. van der Schoot, H. M. Wyss, Micromechanics of temperature sensitive microgels: Dip in the Poisson ratio near the LCST. *Soft Matter* **9**, 7158–7166 (2013).
24. B. R. Saunders, H. M. Crowther, B. Vincent, Poly [(methyl methacrylate)-co-(methacrylic acid)] microgel particles: Swelling control using pH, cononsolvency, and osmotic deswelling. *Macromolecules* **30**, 482–487 (1997).
25. B. Sierra-Martin, J. A. Frederick, Y. Laporte, G. Markou, J. J. Lietor-Santos, A. Fernandez-Nieves, Determination of the bulk modulus of microgel particles. *Colloid Polym. Sci.* **289**, 721–728 (2011).
26. P. Anilkumar, T. B. Lawson, S. Abbina, J. T. A. Mäkelä, R. C. Sabatelle, L. E. Takeuchi, B. D. Snyder, M. W. Grinstaff, J. N. Kizhakkedathu, Mega macromolecules as single molecule lubricants for hard and soft surfaces. *Nat. Commun.* **11**, 2139 (2020).
27. M. Cors, L. Wiehemeier, O. Wrede, A. Feoktystov, F. Cousin, T. Hellweg, J. Oberdisse, Contrast variation SANS measurement of shell monomer density profiles of smart core–shell microgels. *Soft Matter* **16**, 1922–1930 (2020).
28. S. Bergmann, O. Wrede, T. Huser, T. Hellweg, Super-resolution optical microscopy resolves network morphology of smart colloidal microgels. *Phys. Chem. Chem. Phys.* **20**, 5074–5083 (2018).
29. N. Boon, P. Schurtenberger, Swelling of micro-hydrogels with a crosslinker gradient. *Phys. Chem. Chem. Phys.* **19**, 23740–23746 (2017).
30. M. R. Islam, R. Nguyen, L. A. Lyon, Emergence of non-hexagonal crystal packing of deswollen and deformed ultra-soft microgels under osmotic pressure control. *Macromol. Rapid Commun.* **42**, 2100372 (2021).
31. O. Tagit, N. Tomczak, G. J. Vancso, Probing the morphology and nanoscale mechanics of single poly (N-isopropylacrylamide) microgels across the lower-critical-solution temperature by atomic force microscopy. *Small* **4**, 119–126 (2008).
32. S. M. Hashmi, E. R. Dufresne, Mechanical properties of individual microgel particles through the deswelling transition. *Soft Matter* **5**, 3682–3688 (2009).
33. T. Eckert, W. Richtering, Thermodynamic and hydrodynamic interaction in concentrated microgel suspensions: Hard or soft sphere behavior? *J. Chem. Phys.* **129**, 124902 (2008).
34. F. Camerin, N. Gnan, J. Ruiz-Franco, A. Ninarello, L. Rovigatti, E. Zaccarelli, Microgels at interfaces behave as 2D elastic particles featuring reentrant dynamics. *Phys. Rev. X.* **10**, 031012 (2020).
35. L. Rovigatti, N. Gnan, A. Ninarello, E. Zaccarelli, Connecting elasticity and effective interactions of neutral microgels: The validity of the Hertzian model. *Macromolecules* **52**, 4895–4906 (2019).
36. H. Shirota, N. Kuwabara, K. Ohkawa, K. Horie, Deuterium isotope effect on volume phase transition of polymer gel: Temperature dependence. *J. Phys. Chem. B* **103**, 10400–10408 (1999).
37. P. Zavodszky, J. Kardos, Á. Svingor, G. A. Petsko, Adjustment of conformational flexibility is a key event in the thermal adaptation of proteins. *Proc. Natl. Acad. Sci. U.S.A.* **95**, 7406–7411 (1998).
38. M. Chevreuil, D. Law-Hine, J. Chen, S. Bressanelli, S. Combet, D. Constantin, J. Degrouard, J. Möller, M. Zeghal, G. Tresset, Nonequilibrium self-assembly dynamics of icosahedral viral capsids packaging genome or polyelectrolyte. *Nat. Commun.* **9**, 3071 (2018).
39. R. F. Garmann, R. Sportsman, C. Beren, V. N. Manoharan, C. M. Knobler, W. M. Gelbart, A simple RNA-DNA scaffold templates the assembly of monofunctional virus-like particles. *J. Am. Chem. Soc.* **137**, 7584–7587 (2015).
40. K. Zhou, Y. Ke, Q. Wang, Selective in situ assembly of viral protein onto DNA origami. *J. Am. Chem. Soc.* **140**, 8074–8077 (2018).
41. S. Sun, Y. Yang, D. Li, J. Zhu, Large chiral nanotubes self-assembled by DNA bricks. *J. Am. Chem. Soc.* **141**, 19524–19528 (2019).
42. P. Wang, S. Gaitanaros, S. Lee, M. Bathe, W. M. Shih, Y. Ke, Programming self-assembly of DNA origami honeycomb two-dimensional lattices and plasmonic metamaterials. *J. Am. Chem. Soc.* **138**, 7733–7740 (2016).
43. E. Carlon, E. Orlandini, A. L. Stella, Roles of stiffness and excluded volume in DNA denaturation. *Phys. Rev. Lett.* **88**, 198101 (2002).
44. C. Yuan, H. Chen, X. W. Lou, L. A. Archer, DNA bending stiffness on small length scales. *Phys. Rev. Lett.* **100**, 018102 (2008).
45. D. G. Rudmann, J. T. Alston, J. C. Hanson, S. Heidel, High molecular weight polyethylene glycol cellular distribution and PEG-associated cytoplasmic vacuolation is molecular weight dependent and does not require conjugation to proteins. *Toxicol. Pathol.* **41**, 970–983 (2013).
46. L. G. Malito, S. Arevalo, A. Kozak, S. Spiegelberg, A. Bellare, L. Pruitt, Material properties of ultra-high molecular weight polyethylene: Comparison of tension, compression, nanomechanics and microstructure across clinical formulations. *J. Mech. Behav. Biomed. Mater.* **83**, 9–19 (2018).
47. A. Scotti, M. Pelaez-Fernandez, U. Gasser, A. Fernandez-Nieves, Osmotic pressure of suspensions comprised of charged microgels. *Phys. Rev. E* **103**, 012609 (2021).
48. S. Nöjd, P. Holmqvist, N. Boon, M. Obiols-Rabasa, P. S. Mohanty, R. Schweins, P. Schurtenberger, Deswelling behaviour of ionic microgel particles from low to ultra-high densities. *Soft Matter* **14**, 4150–4159 (2018).
49. A. Scotti, M. Brugnoni, C. G. Lopez, S. Bochenek, J. J. Crassous, W. Richtering, Flow properties reveal the particle-to-polymer transition of ultra-low crosslinked microgels. *Soft Matter* **16**, 668–678 (2020).
50. A. Scotti, J. E. Houston, M. Brugnoni, M. M. Schmidt, M. F. Schulte, S. Bochenek, R. Schweins, A. Feoktystov, A. Radulescu, W. Richtering, Phase behavior of ultrasoft spheres show stable bcc lattices. *Phys. Rev. E.* **102**, 052602 (2020).
51. D. B. G. Williams, M. Lawton, Drying of organic solvents: Quantitative evaluation of the efficiency of several desiccants. *J. Org. Chem.* **75**, 8351–8354 (2010).
52. B. Hammouda, D. L. Ho, S. Kline, Insight into clustering in poly (ethylene oxide) solutions. *Macromolecules* **37**, 6932–6937 (2004).
53. M. Brugnoni, A. C. Nickel, L. C. Kröger, A. Scotti, A. Pich, K. Leonhard, W. Richtering, Synthesis and structure of deuterated ultra-low cross-linked poly (N-isopropylacrylamide) microgels. *Polym. Chem.* **10**, 2397–2405 (2019).
54. M. Andersson, S. L. Maunu, Structural studies of poly(*N*-isopropylacrylamide) microgels: Effect of SDS surfactant concentration in the microgel synthesis. *J Polym Sci B* **44**, 3305–3314 (2006).
55. P. L. Hansen, J. A. Cohen, R. Podgornik, V. A. Parsegian, Osmotic properties of poly (ethylene glycols): Quantitative features of brush and bulk scaling laws. *Biophys. J.* **84**, 350–355 (2003).
56. J. J. Lietor-Santos, U. Gasser, R. Vavrin, Z. Hu, A. Fernandez-Nieves, Structural changes of poly (*N*-isopropylacrylamide)-based microgels induced by hydrostatic pressure and temperature studied by small angle neutron scattering. *J. Chem. Phys.* **133**, 034901 (2010).
57. M. Cors, L. Wiehemeier, Y. Hertle, A. Feoktystov, F. Cousin, T. Hellweg, J. Oberdisse, Determination of internal density profiles of smart acrylamide-based microgels by small-angle neutron scattering: A multishell reverse monte carlo approach. *Langmuir* **34**, 15403–15415 (2018).
58. B. Hammouda, D. F. Mildner, Small-angle neutron scattering resolution with refractive optics. *J. Appl. Cryst.* **40**, 250–259 (2007).
59. A. Scotti, A. R. Denton, M. Brugnoni, J. E. Houston, R. Schweins, I. I. Potemkin, W. Richtering, Deswelling of microgels in crowded suspensions depends on cross-link density and architecture. *Macromolecules* **52**, 3995–4007 (2019).
60. A. Scotti, Characterization of the volume fraction of soft deformable microgels by means of small-angle neutron scattering with contrast variation. *Soft Matter* **17**, 5548–5559 (2021).
61. O. L. J. Virtanen, A. Mourran, P. T. Pinard, W. Richtering, Persulfate initiated ultra-low cross-linked poly (*N*-isopropylacrylamide) microgels possess an unusual inverted cross-linking structure. *Soft Matter* **12**, 3919–3928 (2016).
62. I. B. de Aguiar, T. van de Laar, M. Meireles, A. Bouchoux, J. Sprakel, K. Schroën, Deswelling and deformation of microgels in concentrated packings. *Sci. Rep.* **7**, 10223 (2017).
63. T. Höfken, C. Strauch, S. Schneider, A. Scotti, Changes in the form factor and size distribution of nanogels in crowded environments. *Nano Lett.* **22**, 2412–2418 (2022).

Acknowledgments: We acknowledge the use of the free SasView software (www.sasview.org/) for fitting the ellipsoid model and the use of FitIt! for the fits of the form factors (www.github.com/ovirtanen/fitit). We thank M. Burgnoni for the synthesis of the nanogels. **Funding:** We thank the Deutsche Forschungsgemeinschaft within SFB 985—Functional Microgels and Microgel Systems (project no. 191948804), the ERS—OPEN Seed Fund Call 2021 (project no. OPSF630), and MLIN/-AEI/-10.13039/-501100011033/-FEDER,UE (grant no. PID2021-122369NB-100) for financial support. **Author contributions:** A.S. and J.E.H. conceived the project and designed and performed the experiments and data analysis. A.S. led the project. A.S., A.F.-N., and J.E.H. wrote the manuscript. L.F. and J.A. synthesized the deuterated PEG. A.d.l.C., J.R.G., and A.F.-N. performed the osmotic pressure measurements. U.G., A.V.P., and R.S. helped perform the SANS experiments. All authors edited the manuscript. **Competing interests:** The authors declare that they have no competing interests. **Data and materials availability:** All data needed to evaluate the conclusions in the paper are present in the paper and/or the Supplementary Materials. This work is based on experiments performed using the D11 instrument at the Institut Laue-Langevin (ILL), Grenoble, France (doi.ill.fr/10.5291/ILL-DATA.9-11-2067) and using the SANS-I instrument at the Paul Scherrer Institut (PSI), Villigen, Switzerland. All the data used for this study are available at www.radar-service.eu/radar/en/dataset/GGdOLetXbaqYBoDU?token=klEyaRSOdItSEByMropg.

Submitted 8 December 2021
Accepted 13 May 2022
Published 1 July 2022
10.1126/sciadv.abn6129

ScienceAdvances

Resolving the different bulk moduli within individual soft nanogels using small-angle neutron scattering

Judith Elizabeth Houston, Lisa Fruhner, Alexis de la Cotte, Javier Rojo Gonzlez, Alexander Valerievich Petrunin, Urs Gasser, Ralf Schweins, Jrgen Allgaier, Walter Richtering, Alberto Fernandez-Nieves, and Andrea Scotti

Sci. Adv., **8** (26), eabn6129.
DOI: 10.1126/sciadv.abn6129